American Mineralogist, Volume 88, pages 1129–1137, 2003

^{57}Fe Mössbauer-effect studies of Ca-rich, Fe-bearing clinopyroxenes: Part I. Paramagnetic spectra of magnesian hedenbergite

SIGRID G. EECKHOUT[1,2,*] AND EDDY DE GRAVE[2]

[1]Department of Subatomic and Radiation Physics, Ghent University, B-9000 Gent, Belgium
[2]Department of Geology and Soil Science, Ghent University, B-9000 Gent, Belgium

ABSTRACT

Mössbauer spectra (MS) of two natural magnesian hedenbergite samples (hereafter HED1 and HED2) were collected at temperatures in the range 35 to 800 K. At selected temperatures a longitudinal external field of 60 kOe was applied to the absorbers. The samples were observed to order magnetically at $T_N = 33 \pm 1$ K and 27 ± 1 K, respectively. The temperature dependencies of the Fe^{2+} center shifts, δ, were analyzed using the Debye model for the lattice vibrations, including a temperature variation for the intrinsic isomer shift, δ_I. The characteristic Mössbauer temperatures, Θ_M, of HED1 and HED2 were found to be 440 ± 20 K and 490 ± 20 K, and the intrinsic isomer shifts, δ_I, to be 1.434 ± 0.005 mm/s and 1.440 ± 0.005 mm/s, respectively, with a linear correlation coefficient, a, between δ_I and T of -4.5×10^{-5} mm/sK. From the external-field (60 kOe) MS recorded at 83, 147, 223, and 277 K for HED2, the principal component of the electric field gradient (EFG), V_{zz}, is determined to be positive and the asymmetry parameter $0.70 \leq \eta \leq 0.80$. Considering the discrepancy between the calculated and experimental applied-field MS, the obtained results for HED1 are assumed to be somewhat less accurate. The temperature variations of the quadrupole splitting, $\Delta E_Q(T)$, have been interpreted using the crystal-field model. Two approaches have been applied to evaluate the crystal field. In both cases the crystal-field Hamiltonian included the spin-orbit coupling. The first model emanates from the approximate and simplified symmetry of the ferrous sites, whereas the second takes into account the real symmetry of the sites, thus leading to a point-charge calculation. The temperature variations $\Delta E_Q(T)$ and $\eta(T)$ could be successfully described using the latter approach.

INTRODUCTION

Ca-rich clinopyroxenes (monoclinic, space group $C2/c$) have been the subject of numerous mineralogical and spectroscopic investigations. In this first of three papers reporting on extensive and detailed Mössbauer studies of near-end-members along the hedenbergite–diopside join, the results and interpretations of the Mössbauer spectra of two magnesian hedenbergite species are presented. Part two focuses on the magnetic characteristics of these hedenbergite samples, while the third and last contribution deals with the Mössbauer spectroscopic features of diopside (three samples with different Fe contents).

In hedenbergite, ideally $CaFe^{2+}Si_2O_6$, Ca^{2+} cations occupy the strongly deformed M2 polyhedra with eightfold O atom coordination, whereas the more regular octahedral M1 sites contain Fe^{2+} (Cameron et al. 1973). In principle, hedenbergite should give rise to a single well-resolved quadrupole doublet at T exceeding the Néel temperature, T_N (Amthauer and Rossman 1984; Stanek et al. 1986; Redhammer et al. 2000; Tennant et al. 2000). Since naturally occurring hedenbergite is almost never ideal in composition, fluctuations in the chemical environment of the ^{57}Fe probes and/or the presence of ferric ions will produce additional subspectra. Consequently, reported paramagnetic Mössbauer spectra (MS) for natural samples have been decomposed into several quadrupole doublets due to Fe^{2+} at M1 sites (Amthauer and Rossman 1984; Stanek et al. 1986; Redhammer et al. 2000; Tennant et al. 2000), Fe^{2+} at M2 sites (Bancroft et al. 1971; Dowty and Lindsley 1973), and Fe^{3+} at M1 sites (Dollase and Gustafson 1982; Amthauer and Rossman 1984; Redhammer et al. 2000). In the solid-solution-series member acmite–hedenbergite (50–50%) ($Na_{0.5}Ca_{0.5}Fe_2Si_2O_6$) and in the hedenbergite-aegirine ($CaFe^{2+}Si_2O_6$-$NaFe^{3+}Si_2O_6$) solid-solution series inter-site electron hopping between Fe^{2+} and Fe^{3+} at the M1 sites has been observed (Amthauer et al. 1998; Redhammer et al. 2000).

In this paper a detailed variable-temperature Mössbauer spectroscopic study, providing important information on lattice temperatures, electronic structures, and geometrical distortions of the distinct iron sites, is presented. Two well-characterized, natural, magnesian hedenbergite samples were considered. Only temperatures exceeding the respective Néel temperatures were dealt with. Similar studies of hedenbergite are very scarce in the literature. To the best of the authors' knowledge, only the temperature variations of the asymmetry parameters for two natural hedenbergite samples have been reported (Stanek et al. 1986).

EXPERIMENTAL METHODS

Two natural hedenbergite samples were investigated: dark-green needles from Elba and nearly black needles from Lemhi County, Idaho, hereafter called HED1 and HED2 respectively. Powder X-ray diffraction data (Philips PW1730/10 diffractometer) indicated that each sample was single-phase hedenbergite.

* E-mail: sigrid.eeckhout@rug.ac.be

Results of the electron microprobe analyses (JSM-6400 SEM and JXA-6400 microprobe), combined with the evaluation of the Fe^{2+}/Fe^{3+} ratio from Mössbauer data (see below) lead to the following compositional formulae:

HED1: $Ca_{1.00}Fe^{2+}_{0.74}Mg_{0.16}Mn_{0.03}Al_{0.03}Fe^{3+}_{0.02}Si_{2.00}O_{6.00}$

and

HED2: $Ca_{1.00}Fe^{2+}_{0.68}Mg_{0.20}Mn_{0.15}Al_{0.05}Fe^{3+}_{0.04}Si_{1.92}O_{6.00}$.

According to the classification scheme proposed by Morimoto (1988), HED1 is magnesian hedenbergite and HED2 a magnesian, manganoan hedenbergite.

MS were collected in transmission geometry using a $^{57}Co(Rh)$ source with a conventional, constant-acceleration drive and triangular reference signal. The temperature was varied between 35 and 800 K in steps of 20 K on average. Low (down to 35 K) and high (up to 800 K) temperatures were obtained using standard commercial cryogenic and heating equipment available in the laboratory. The absorbers had a thickness of approximately 10 mg/cm^2 of natural Fe and counts were accumulated in 1024 channels. The accumulation of data was continued until an off-resonance count of ~10^6 was reached. The velocity scale was periodically calibrated using the MS of a standard α-Fe absorber at room temperature. The velocity increment per channel was ~0.015 mm/s. All center-shift values quoted hereafter are relative to α-Fe. At selected temperatures, viz., at 80, 150, 230, and 290 K for HED1 and at 83, 147, 223, and 277 K for HED2, MS were collected in an external magnetic field of 60 kOe, applied parallel to the incident γ-ray beam. The magnetic order-disorder transition temperature, T_N, was determined by measuring the temperature variation of the transmission of γ-rays through the absorber with the source at zero velocity, the so-called thermoscanning method (Chambaere and De Grave 1984).

MAGNETIC ORDER-DISORDER TRANSITION TEMPERATURE

The magnetic order-disorder transition temperature, T_N, was found to be 33 ± 1 K for HED1 and 27 ± 1 K for HED2, which is within the range found earlier for both synthetic (Coey and Ghose 1985; Ghose et al. 1988) and natural (Stanek et al. 1986; Wiedenmann and Regnard 1986; Regnard and Boujida 1988; Baum et al. 1997) hedenbergites. As expected with increasing diamagnetic dilution, e.g., by Mg, T_N decreases from 38 K for synthetic hedenbergite (Coey and Ghose 1985; Ghose et al. 1988) to 28 K for natural $Ca_{0.97}Fe_{0.79}Mg_{0.06}Mn_{0.17}Al_{0.01}Si_{2.00}O_{6.01}$ (Stanek et al. 1986).

SPECTRAL ANALYSES AND RESULTS

Zero-field MS

The MS collected in zero external magnetic field at $T \geq T_N$ (see Fig. 1 for HED2) consist of two dominant absorption lines, at velocities of ~–0.2 mm/s and ~2.6 mm/s at 80 K, arising from ferrous ions, and a weak, broad absorption line at ~0.8 mm/s due to Fe^{3+}. The low-velocity ferric absorption line is obviously not resolved. In a first attempt, the MS were fit with a discrete number of symmetrical Lorentzian doublets (i.e., each doublet showing equal widths and line intensities for the two partner lines), without imposing any additional restrictions on the parameter values to be adjusted. This Lorentzian model was applied using one ferrous and one ferric doublet or using two ferrous and one ferric component. All attempts in that respect failed in that unrealistic temperature variations for the resulting center shifts, δ, and relative spectral areas, *RA*, were obtained. Therefore, the discrete-doublet approach was abandoned and, in what follows, the results of the Lorentzian model will not be considered.

Visual inspection of the HED2 spectra reveals a slightly asymmetric peak depth for the low- and high-velocity components of the dominant doublet, the positive-velocity peak exhibiting slightly higher absorption intensity. Possible causes for this kind of asymmetry are texture effects due to preferred orientations of the crystallites in the absorber, and non-uniform next-nearest-neighbor (NNN) cationic configurations around the probe Fe nuclei. The importance of texture can be ruled out since the RT MS, collected with the respective absorber planes held at the magic angle (~54°) with respect to the incident γ-beam, exhibit the same asymmetry features, which would not be the case if texture would lie on the basis of the asymmetry (Nagy 1978).

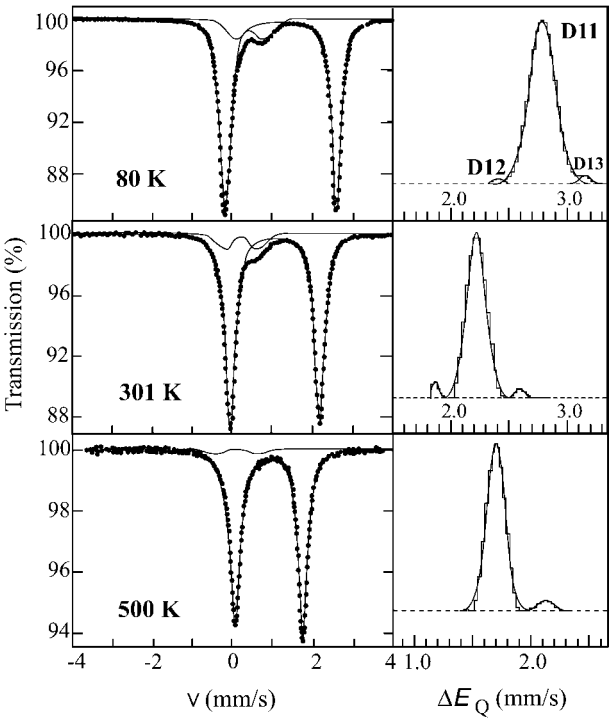

FIGURE 1. Experimental (dots) and calculated (solid lines) Mössbauer spectra and corresponding ferrous quadrupole-splitting, ΔE_Q, distribution profiles at selected temperatures for HED2.

In the next stage of the numerical-analysis process, the effects of the non-uniform NNN configurations were considered. As has been demonstrated by Seifert (1983) for aluminous orthopyroxene, and more recently by Eeckhout et al. (2000) for synthetic $P2_1/c$ Mg-Fe clinopyroxenes, NNN interactions may play an important role in affecting the hyperfine parameters of the central ^{57}Fe probe. Considering the multi-elemental compositions of the hedenbergite species, it was believed that a discrete distribution pattern, with probabilities of the various NNN cation configurations governed by the binomial law, would not be effective. Instead, a more or less broad, quasi-continuous distribution of values for the hyperfine parameters seems to be more conceivable. The use of shape-independent distributions seems to be appropriate and the concept has been applied successfully to many natural systems, including pyroxene minerals such as Fe-bearing aluminum diopsides (De Grave et al. 2002) and amphibole minerals such as riebeckites (Van Alboom and De Grave 1996).

With this idea in mind, the MS of HED1 and HED2 were

interpreted in terms of superpositions of two model-independent quadrupole-splitting distributions (QSD), one for Fe^{2+} (D1) and one for Fe^{3+} (D2). The iteration procedure is based on the mathematical formulation of Wivel and Mørup (1981), later worked into a versatile fitting method for MS with distributed hyperfine-interaction parameters (Amarasiriwardena et al. 1986; Vandenberghe et al. 1994). Each QSD had a single, but different, center-shift value for the elemental doublets. The ΔE_Q range for the Fe^{3+} QSD was chosen to extend from 0.00 to 1.30 mm/s for HED1 and HED2, both increasing in steps of 0.05 mm/s. Since ΔE_Q for Fe^{2+} is generally strongly temperature dependent, the upper and lower limits for the QSD range were lowered with increasing temperatures, i.e., 3.30 and 2.30 mm/s for the MS at 36 K, and 1.80 and 0.80 mm/s for the MS at 800 K, respectively. At each temperature, a total of 34 subdoublets were calculated in steps of 0.03 mm/s for ΔE_Q. The adjustable parameters were δ, a linear correlation coefficient, $C_{\delta,Q}$, between δ and ΔE_Q, and the width Γ of the elemental Lorentzian doublets. Due to the weak spectral contribution of the D2 component and to the strong overlap with the D1 component for temperatures $T > 450$ K for HED1 and $T > 500$ K for HED2, only one single contribution (D1) was iterated for these temperatures.

Results of the applied fitting procedure for HED2 are shown in Figure 1 and the relevant Mössbauer parameters for the different subspectra at some selected temperatures are listed in Table 1. The goodness-of-fit functions, χ^2, for the QSD fits are generally lower than the corresponding values for the discrete-doublet fits, but not substantially.

The fractional areas of ferric D2 for HED1 are ~0.02 and hence its parameters are ill defined. Moreover, as suggested by Stanek et al. (1986), who observed a similar component in their hedenbergite MS, this ferric contribution may arise from a strongly intergrown impurity phase. To check this proposition, additional MS on another piece of the HED1 needle-like aggregate were collected. The RT MS showed a somewhat greater contribution of the ferric component, thus to some extent supporting the above-made conclusion. However, no further attention will be devoted to the D2 component resolved from the HED1 MS.

As for the D1 component, its QSD profile clearly shows a predominant contribution and one or two additional, minor satellite peaks, indicated as D12 and D13 in Figure 1. Although the maximum-probability quadrupole-splitting values $\Delta E_Q{}^m$ for the satellites (which are more relevant than the average quadrupole splittings since the latter depend on the selected upper and lower limits of the distribution) of 2.36 and 3.11 mm/s at 80 K, and center-shift values δ^m of ~1.30 mm/s are not uncommon for Fe^{2+} in octahedral O atom environments in silicate minerals (e.g., Dowty and Lindsley 1973; Amthauer and Rossman 1984; Stanek et al. 1986), their origin remains puzzling. It could be that their presence reflects the NNN effect mentioned above. However, since it is unlikely that M2 sites are occupied by cations other than Ca^{2+}, the effect would arise from different configurations of the more distant M1 neighbors. It is hard to imagine that these different configurations would induce such large shifts in the quadrupole splitting. Moreover, the relative contributions of D12 and D13 to the total D1 component (~5% each) seem to be too low to be consistent with the binomial probabilities estimated from the elemental composition of HED1.

The results for HED2 are quite similar to those for HED1, except that the ferric D2 component is present to a greater extent, and hence its Mössbauer parameters obtained from the fitting procedure are more reliable. The QSD profiles for D2 show no structure and are quite symmetric around the respective maximum-probability values listed in Table 1. These values are not diagnostic and similar data are found for several other silicates, and even oxides. The D1 component again is composed of a major peak and one or two satellite peaks, the nature of which are, as in the case of HED1, unclear. The relevant Mössbauer parameters (Table 1) of the dominant contribution to the D1 QSD are almost identical to the values for HED1.

At one stage in this research the authors had the idea that the ferric component D2 might be due partly to an oxide layer covering the hedenbergite grains. To check this out, the HED2 powder was treated with diluted HCl and thoroughly washed afterward. Powder X-ray diffraction data confirmed that the hedenbergite structure had remained unaltered, while MS showed that the fractional area *RA* of D2 was diminished after treatment, with no measurable effect on the D1 parameters. This could indicate that a portion of the D2 component might be attributable to a surface impurity phase of the HED2 needle-like aggregates, while another portion is due to Fe^{3+} at the octahedral sites of the hedenbergite structure. No further evidence

TABLE 1. Mössbauer parameters of HED1 and HED2 at some selected temperatures

HED 1					HED 2									
D1					D1						D2			
T	$\Delta E_{Q,D1}{}^m$	δ^m	$C_{\delta,Q}$	Γ	T	$\Delta E_{Q,D1}{}^m$	δ^m	$C_{\delta,Q}$	Γ	*RA*	$\Delta E_{Q,D2}{}^m$	δ	Γ	*RA*
36	2.72	1.311	0.106	0.31	36	2.72	1.304	0.049	0.26	0.86	0.67	0.55	0.29	0.14
50	2.73	1.310	0.033	0.26	49	2.76	1.303	0.065	0.26	0.87	0.64	0.55	0.27	0.13
80	2.74	1.304	0.060	0.27	80	2.76	1.294	0.048	0.24	0.86	0.66	0.51	0.28	0.14
140	2.65	1.279	0.059	0.28	140	2.66	1.276	0.015	0.25	0.87	0.64	0.55	0.35	0.13
200	2.50	1.244	0.049	0.29	200	2.52	1.240	0.054	0.25	0.88	0.69	0.50	0.33	0.12
300	2.19	1.179	0.060	0.29	301	2.21	1.180	0.081	0.26	0.90	0.68	0.34	0.22	0.10
400	1.90	1.110	0.153	0.27	400	1.94	1.117	0.151	0.26	0.96	0.72	0.37	0.22	0.04
521	1.60	1.024	0.293	0.26	500	1.69	1.046	0.168	0.26	0.97	0.91	0.23	0.22	0.03
650	1.33	0.923	0.301	0.26	650	1.38	0.936	0.325	0.26	1.00				
800	1.11	0.804	0.318	0.24	800	1.12	0.804	0.263	0.27	1.00				
Error	0.01	0.005	0.005	0.01		0.01	0.005	0.005	0.01	0.01	0.08	0.04	0.04	0.01

Notes: Temperature T(K), quadrupole splitting ΔE_Q(mm/s), center shift δ (mm/s, relative to α-Fe), line width Γ (mm/s), and relative spectral area *RA* of elemental doublet. The superscript m refers to the maximum-probability values and $C_{\delta,Q}$ is the linear correlation coefficient between δ and ΔE_Q.

or indication that this suggestion is true was found in the course of this research. The data listed in Table 1 refer to the treated sample.

Applied-field MS

The applied-field MS (AFMS) of HED1 and HED2 at selected temperatures and subjected to a field of 60 kOe are reproduced in Figure 2. They were interpreted taking into account several subspectra for each component (D1 and D2) corresponding to discrete values for the polar and azimuthal angles θ and φ of the external field with respect to the principal-axes frame of the EFG (θ being the angle with the *Z* axis), and adjusting the superposition of these subspectra to the observed AFMS. Twelve values for φ were considered and twenty values for θ, the latter with a $\sin^2\theta$ probability distribution (so-called "summation over the unit sphere"). Hence, a total of 240 (HED1) and 480 (HED2, including the Fe^{3+} contribution) components were evaluated. The parameters of each elemental component were calculated by diagonalization of the complete hyperfine-interaction Hamiltonians (HIH). For Fe^{2+} species in a non-cubic environment, an anisotropic field reduction due to spin polarization (Varret 1976a) has to be taken into account. In addition to δ, ΔE_Q, and Γ, the asymmetry parameter η of the EFG, and the field reductions *HIX, HIY,* and *HIZ* were fitted. These latter quantities, when subtracted from the external-field value, yield the effective hyperfine fields, which would be observed for a single crystal if the external field were applied along the EFG principal axes *X*, *Y*, and *Z*, respectively. In case of Fe^{3+}, which has isotropic magnetic properties, one field-reducing parameter, H_{red}, has to be considered. For HED1, only the ferrous component was considered, while for HED2, both the ferrous and ferric component were taken into account, however with several constraints. The *RA* of both components and δ of D2 were kept fixed at the values obtained for the zero-field paramagnetic MS at the same *T*, and η of D2 was fixed at 0.

The full lines in Figure 2 represent the line shapes calculated on the basis of the complete HIH. In general, the agreement with the observed line shapes is reasonable. The adjusted parameters are listed in Table 2. The values for δ and ΔE_Q are in excellent agreement with those iterated from the zero-field MS. For HED1 the EFG principal component, V_{zz}, was found to be negative, while for HED2 it is positive. This would mean that the first-order deformations of the octahedral symmetry of the M1 sites in HED1 and HED2 are significantly different.

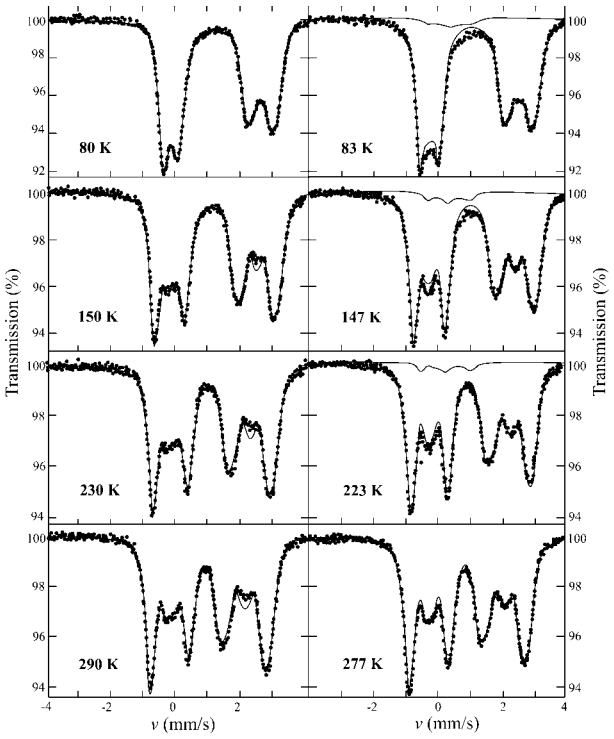

FIGURE 2. Experimental (dots) and calculated (solid lines) Mössbauer spectra obtained at different temperatures in an external magnetic field of 60 kOe for HED1 (left side) and HED2 (right side).

More precisely, considering the magnitude of ΔE_Q, which indicates an orbital singlet ground state for the Fe^{2+} ions, a trigonal compression for M1 in HED1 and a tetragonal compression for M1 in HED2 (Ingalls 1964) was found. It is surprising that such relatively small changes in the elemental compositions can cause such a drastic effect on the M1-site geometry. However, one needs to be cautious and critical in this respect. For both hedenbergite species the asymmetry parameter, η, is rather high. This is obvious from the fine structure of the low- and high-velocity triplets (Collins and Travis 1967). In such cases the sign of V_{zz} is ill defined. It indeed changes when η surpasses the value of 1.00. Anyway, the high η values imply that the geometries and/or the surrounding charge distributions of the Fe^{2+}(M1) sites are strongly deformed from axial symmetry.

TABLE 2. Some relevant results derived from the applied-field (60 kOe) MS at various temperatures

Sample	*T*	δ	ΔE_Q	SGN(V_{zz})	η	Γ	*HIX*	*HIY*	*HIZ*
HED1	80	1.30	2.75	–	0.81	0.34	–37	–21	–42
	150	1.27	2.64	–	0.86	0.32	–20	–10	–25
	230	1.22	2.43	–	0.93	0.32	–12	–7	–19
	290	1.17	2.25	–	0.99	0.32	–7	–4	–15
HED2	83	1.29	2.76	+	0.70	0.33	–33	–41	–21
	147	1.26	2.66	+	0.78	0.31	–21	–21	–10
	223	1.22	2.45	+	0.72	0.30	–12	–13	–7
	277	1.17	2.29	+	0.80	0.30	–10	–11	–5
Error		0.02	0.04		0.15	0.02	2	2	2

Notes: Temperature *T* (K), center shift δ (mm/s, relative to α-Fe), quadrupole splitting ΔE_Q (mm/s), sign of the principal component of the electric field gradient SGN(V_{zz}), line width Γ (mm/s), components of the anisotropic reduction field *HIX, HIY,* and *HIZ* (kOe).

Since the field reductions *HIX* and *HIY* have similar values, the magnetization axis lies on the bisectrice plane of the *XY* plane of the principal-axes frame of the EFG. The somewhat smaller value for *HIZ* reveals that the magnetization axis makes a small angle with the *XY* plane of the principal-axes frame of the EFG.

Stanek et al. (1986) studied two hedenbergite minerals in the *T* range 4.2–295 K and under applied fields of 4.5–7.5 T. For the sample with composition $Ca_{0.97}Mn_{0.17}Fe_{0.79}Mg_{0.06}Al_{0.01}Si_{2.00}O_{6.01}$ these authors obtained at 295 K a negative sign for V_{zz} and $\eta \approx 0.6$. For $Ca_{0.96}Mn_{0.02}Fe_{0.66}Mg_{0.31}Al_{0.06}Si_{1.99}O_{6.02}$ at 295 K a negative V_{zz} and $\eta = 1.0$, and at 78 K a positive V_{zz} and $\eta = 0.3$ were found. For the former sample, the largest value for the field reduction occurs along the *Z* axis, in accordance with the present findings, and for the latter one along the *Y* axis. Tennant et al. (2000) obtained for a single crystal of hedenbergite with Fe content of ~0.54 atoms per formula unit a negative V_{zz} and $\eta = 0.97$. In summary, it is obvious that reported results concerning the sign and the asymmetry of the EFG are to some extent in disagreement. The sign of V_{zz} is reported to be either positive or negative, and a reversal of that sign at some temperature is possible. According to the present results, when $V_{zz} > 0$, the largest value for the field reduction is that along the *Y* axis of the principal-axes frame of the EFG, while if $V_{zz} < 0$ *HIZ* seems to be the highest. The reason for this behavior is unclear; perhaps the composition plays a crucial role.

DISCUSSION

Temperature dependence of the Fe^{2+} center shifts

The observed temperature variations of the Fe^{2+} center shifts for HED1 and HED2 are reproduced in Figure 3. Considering the minor contributions of the ferric components, and hence their ill-defined parameter values, these components have not been considered for further interpretation of the observed hyperfine interactions.

Generally, the center shift, δ, consists of a contribution arising from the *s*-electron density at the ^{57}Fe nucleus, δ_I, and a contribution due to the non-zero mean square velocity of the nucleus, the so-called second-order Doppler shift, δ_{SOD}, which is significantly dependent upon temperature. Commonly, $\delta(T)$ is interpreted on the basis of the following expression:

$$\delta(T) = \delta_I + \delta_{SOD}(T). \quad (1)$$

The intrinsic isomer shift, δ_I, is weakly dependent upon *T*, due to the thermal radial expansion of the t_{2g} and e_g wave functions. This dependence, however, can only be noticed if sufficient data at temperatures exceeding ~500 K data are available (De Grave and Van Alboom 1991). The second-order Doppler shift, δ_{SOD}, is related to the vibrational properties of the probe nuclei in the crystal structure. Usually, the Debye approximation for the lattice vibrational spectrum provides an adequate model for calculating $\delta_{SOD}(T)$. In this model, one parameter, the so-called characteristic Mössbauer temperature or lattice temperature, Θ_M, appears in the mathematical formulation. The adjusted curves in Figure 3 (solid lines) were obtained in this manner and clearly show an excellent agreement with the observed data at $T \leq 600$ K. The calculated Θ_M are 330 ± 20 K and 370 ± 20 K for HED1 and HED2, respectively (see Table 3). This implies that chemical bonding at the octahedral sites is similar for the two hedenbergite species and that there is little influence of substitutions at M1 upon the Mössbauer temperature.

At temperatures above 600 K, the calculated $\delta(T)$ values slightly, but consistently, exceed the experimental data. This implies that at such high temperatures $\delta_{SOD}(T)$ is not able to describe $\delta(T)$ adequately. Perkins and Hazony (1972) obtained similar results for their $\delta(T)$ curves observed for some iron halogenides and proposed a weak temperature dependence of the form:

$$\delta_I(T) = \delta_I(0\ K) + C_{\delta,Q} \times 10^{-5}\ T \quad (2)$$

to explain the mismatch between the observed and calculated $\delta(T)$ values. These authors argue that this temperature dependence is due to the thermal radial expansion of the t_{2g} and e_g wave functions. To obtain Θ_M values for the present hedenbergite species, Equation 2 was used with no constraints imposed on the linear correlation coefficient, $C_{\delta,Q}$. A closer agreement between the experimental and calculated data is obvious, particularly at $T \geq 600$ K (Fig. 3, dashed lines). Θ_M was found to be 440 ± 20 K for HED1, and 490 ± 20 K for HED2 (see Table 3), and the linear correlation coefficient was -4.5×10^{-5} mm/s.K. These Θ_M values are ~100 K higher than in the case where no temperature variation for δ_I was considered. This is conceivable since the temperature dependence of δ_I also has an effect, although to a lesser extent, at relatively "low" temperatures in a way that, if the correlation is not intro-

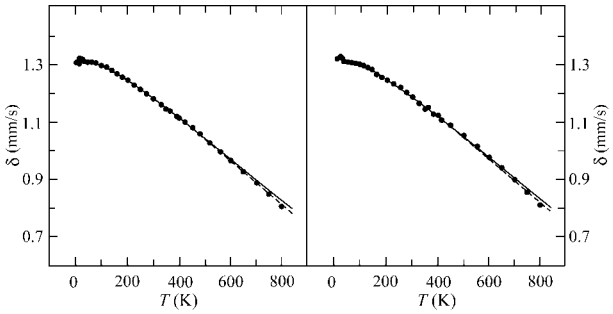

FIGURE 3. Experimental and calculated (solid lines) temperature dependence of the ferrous center shifts, $\delta(T)$, for HED1 (left side) and HED2 (right side). The calculated $\delta(T)$ curves when including a linear correlation coefficient, α, between the intrinsic center shift, δ_I, and the temperature, *T*, (dashed lines) are shown as well.

TABLE 3. Characteristic Mössbauer temperature Θ_M (K), intrinsic isomer shift δ_I (mm/s), a linear correlation coefficient $C_{\delta,Q}$, and Mössbauer fraction f_2 at 80 K of Fe^{2+} in HED1 and HED2

Sample	Θ_M	δ_I	$C_{\delta,Q}$	f_2
HED1	330	1.406	0	0.87
	440	1.434	–4.5	0.91
HED2	370	1.411	0	0.89
	490	1.440	–4.5	0.92
Error	20	0.005		0.01

duced in the model, $\delta_{SOD}(T)$ has to take account of a steeper decrease of $\delta(T)$ with increasing temperature, thus yielding a lower value for Θ_M. However, this finding is the same for the two minerals and for other silicates (De Grave and Van Alboom 1991; see Part III of these studies) and does not affect the above conclusions with respect to the chemical-bond properties.

The ferrous Mössbauer fractions, f_2, at 80 K calculated from these Θ_M values (De Grave and Van Alboom 1991) are 0.91 and 0.92 for HED1 and HED2, respectively. Hence, the Fe^{2+} recoil-free fractions for both samples are equal within the error.

Temperature dependence of the Fe^{2+} quadrupole splittings

The temperature variations of the Fe^{2+} quadrupole splittings, $\Delta E_Q(T)$, for HED1 and HED2 are depicted in Figures 4a and 4b, respectively. In order to explain quantitatively the observed $\Delta E_Q(T)$ curves, the ferrous valence contribution was calculated within the crystal-field model from the Boltzmann populations of the electronic levels within the ^5D term and the expectation values of the EFG components for these ^5D levels. Two different methods were applied, the first based on an approximation for the local symmetry of the M1 sites, the second using the real symmetry as manifested by point-charge calculations, and subsequently diagonalization of the complete crystal-field Hamiltonian.

According to the crystallographic data determined by Cameron et al. (1973), the M1 coordinations of hedenbergite can schematically be represented as in Figure 5. These representations show a so-called *case 2* of orthorhombic symmetry (Varret 1976b) to which the local symmetry can be simplified. In this case the splitting of the electronic levels within the ^5D term is as depicted in Figure 6. As mentioned previously, the second approach for evaluating $\Delta E_Q(T)$ concerns a point-charge calculation and consequently accounts for the real local symmetry of the M1 site. The proper ^5D level schemes were determined by diagonalization of the full crystal-field Hamiltonian. The lattice contribution was obtained from lattice summation. For a more detailed description of the applied methods, the reader is referred to Van Alboom et al. (1993).

The solid lines in Figure 4 represent the fitted $\Delta E_Q(T)$ curves based on the crystal-field approximation and assuming *case 2* of the orthorhombic symmetry for the M1 site. For the interpretation of $\Delta E_Q(T)$ it is desirable to have some complimentary information about the level scheme of the ferrous ^5D ground term. These data can be retrieved from optical absorption spectra. Such spectra for hedenbergite consist of two broad bands centered at 8475 cm^{-1} and 10 200 cm^{-1}, which correspond to the third, Δ_3, and fourth, Δ_4, excited orbital states with respect to the ground state (Burns 1993). From these data the upper limit of the cubic level splitting of the ^5D ground term in an octahedral crystal field, Δ_{oct} (Fig. 6), is estimated to be ~9400 cm^{-1}. The relative positions of the T_{2g} levels can only be estimated from fitting the theoretical $\Delta E_Q(T)$ expressions to the experimental curves. The values of the crystal-field coefficients B_{20} and B_{22}, which quantify the energy gaps between the three lowest electronic levels of the T_{2g} orbitals (Fig. 6), and of the quadrupole-splitting-coupling constant, ΔE_0, need to be adjusted. The lattice contribution to the EFG was expressed in

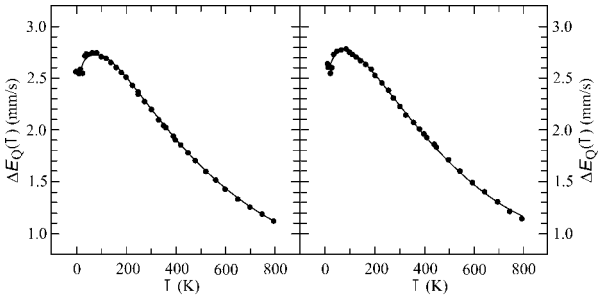

FIGURE 4. Experimental and calculated (solid lines) temperature dependence of the ferrous center shifts, $\delta(T)$, for HED1 (left side) and HED2 (right side). The calculations are based on the crystal-field approximation and assuming *case 2* of the orthorhombic symmetry for the M1 site.

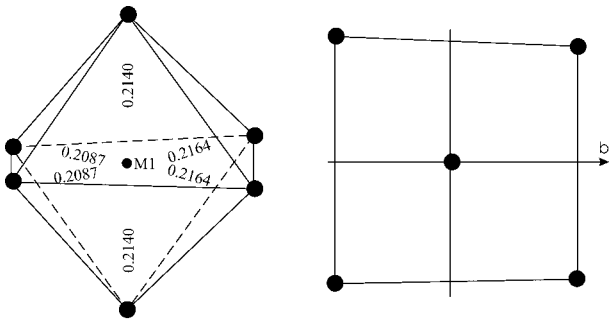

FIGURE 5. Perspective representation (M-O distances in nm; left side) and projection along the connection line of the apical O ions onto the normal plane (right side) of the M1 site in hedenbergite.

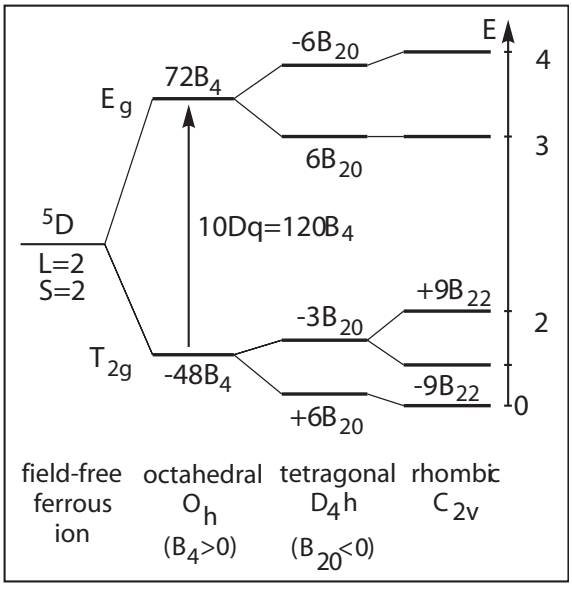

FIGURE 6. Level scheme of the ferrous ^5D ground term assuming *case 2* of the orthorhombic symmetry. Δ_i is the level splitting of the i^{th} excited orbital level or of the barycenter of that level accounting for the spin-orbit interaction, with respect to the ground level.

terms of B_{20} and B_{22} (Ingalls 1964). The maximum-probability quadrupole-splitting values (Table 1) were used as experimental data.

Around 80 K, both samples exhibit a maximum in the $\Delta E_Q(T)$ curve, implying that the effect of the spin-orbit interaction, λ**L.S** (with **L** and **S** the orbital and spin vector operators), is not negligible for the studied magnesian hedenbergites. An additional problem concerns the unknown magnitude of the spin-orbit-coupling constant, λ, within the FeO_6^{10-} clusters in hedenbergite. To the best of our knowledge, no literature data are available in that respect. Hence the value of λ had to be derived from the observed data, which was established by trial and error, implying that this value is not very accurate and at best a first approximation. To make the theoretical treatment complete, the Heisenberg spin-spin-interaction Hamiltonian was additionally included in the final calculations for temperatures below the respective Néel temperatures. This Hamiltonian has the form $H_{ss} = 2zJ_{eff}<\mathbf{S}_j>.\mathbf{S}_i$ (Morrish 1965) with z the number of magnetic first neighbors of the probe nucleus, $\mathbf{S}_i$ its spin operator, $<\mathbf{S}_j>$ the average spin of the surrounding magnetic ions, and J_{eff} the effective magnetic exchange integral.

Initial values for the crystal-field coefficients B_{20}, B_{22}, and for ΔE_0 were estimated from the temperature variation of ΔE_Q in the range $T > 80$ K. The spin-orbit-coupling was not included in these preliminary calculations. The initial value for the isotropic exchange integral was derived from the relation (Morrish 1965)

$$\frac{zJ_{eff}}{k} = \frac{3\theta_P}{2S(S+1)} \quad (3)$$

in which θ_P represents the paramagnetic Curie temperature. Using $\theta_P = 21$ K, as measured by Regnard and Boujida (1988) and by Baum et al. (1997) for a sample with a comparable Fe content, one obtains $\frac{zJ_{eff}}{k} = 5.25$ K. In subsequent calculations λ was kept fixed, however its value was adjusted to some extent by trial and error to obtain the best agreement between the experimental and calculated $\Delta E_Q(T)$ curves. A value of $\lambda = -60 \pm 5$ cm^{-1} seemed to be adequate. It is important to note that during iterative calculations the B_4 coefficient was chosen such that the mean calculated position of the E_g levels was 9400 cm^{-1}, which is the estimated upper limit for Δ_{oct} (see above). Results of the applied procedure are given in Table 4. As generally accepted, the valence and lattice contributions are of opposite sign (Ingalls 1964) and the lattice term is small. The negative value for B_{20} is consistent with the aforementioned conclusion that Fe^{2+} at M1 exhibits a singlet electronic ground state (Ingalls 1964).

The temperature variations of the asymmetry parameter for HED1 and HED2 as obtained from the above calculations are depicted in Figure 7, together with the experimental values determined in this work and those reported by Stanek et al. (1986). Visual inspection of Figure 7 clearly reveals that h(T) cannot properly be described by this model. Furthermore, the approach resulted in a positive sign for V_{zz} at each T, even for HED1. Stanek et al. (1986) described h(T) of natural $Ca_{0.96}Fe_{0.66}Mg_{0.31}Mn_{0.02}Al_{0.06}Si_{1.99}O_{6.02}$ using the crystal-field approximation assuming *case 1* of the orthorhombic symmetry for the M1 site (Varret 1976b) and neglecting spin-orbit coupling. The as-such calculated energies of the first and second excited orbital states with respect to the ground state were found as $\Delta_1 = 130$ cm^{-1} and $\Delta_2 = 565$ cm^{-1}, respectively. Since the value for Δ_1 has the same order of magnitude as the spin-orbit-coupling constant for the free Fe^{2+} ion, the latter effect is, however, not negligible. As a test, the level scheme of Stanek et al. (1986) was used as initial guess for the interpretation of the $\eta(T)$ and $\Delta E_Q(T)$ data reported by these authors and assuming *case 1* of the orthorhombic symmetry. Although the experimental $\eta(T)$ curve was satisfactorily described by the model, the calculated $\Delta E_Q(T)$ curve was strongly and unacceptably deviating from the observed variation. This finding is in the present authors' opinion a strong indication that the proposed level scheme is inadequate, the energies of the excited electronic levels being grossly underestimated. Obviously, the crystal-field model presented above and based upon an

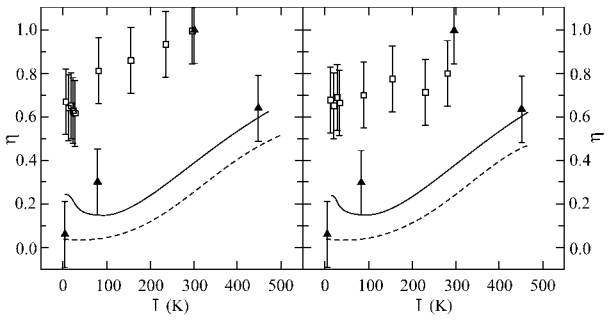

FIGURE 7. Experimental (open box this study, filled triangle Stanek et al. 1986) and calculated (dashed lines) temperature dependence of the asymmetry parameter $\eta(T)$ assuming *case 2* of the orthorhombic symmetry for HED1 (left side) and HED2 (right side). The calculated $\eta(T)$ curves when including the spin-orbit-coupling constant λ (solid lines) are shown as well.

TABLE 4. Results concerning the ^5D level scheme and the electric field gradient EFG for Fe^{2+} in HED1 and HED2 as obtained from the temperature variation of the quadrupole splitting based on case 2 of the hypothetical orthorhombic symmetry for the M1 site

Sample	B_{20}	B_{22}	λ	ΔE_0	α^2	$\Delta E_{Q,lat\ q}$	$\Delta E_{Q,lat\ \eta}$	η	Δ_{oct}	Δ_1	Δ_2	Δ_3	Δ_4
HED1	–77.9	–10.2	0	2.92	0.78	–0.20	–0.25	0.04	8920	410	1010	8930	9880
	–67.2	–90.3	–60	3.26	0.86	–0.17	–0.23	0.15	8930	380	950	8990	9810
HED2	–80.3	–106.4	0	2.94	0.78	–0.20	–0.27	0.04	8890	420	1060	8910	9880
	–69.3	–95.9	–60	3.27	0.87	–0.17	–0.24	0.15	8920	400	980	8980	9820

Notes: B coefficient, i.e., B_{20} and B_{22} (cm^{-1}), spin-orbit-coupling constant λ (cm^{-1}), quadrupole-coupling constant ΔE_0 (mm/s), covalence factor α^2, lattice contributions $\Delta E_{Q,lat\ q}$ and $\Delta E_{Q,lat\ \eta}$ (mm/s), asymmetry parameter η at 80 K, cubic level splitting of the ^5D ground term in an octahedral crystal field Δ_{oct} (cm^{-1}), first Δ_1, second Δ_2, third Δ_3, and fourth Δ_4, excited orbital state with respect to the ground state (cm^{-1}).

orthorhombic *case 2* model is a fairly good approximation for the Fe^{2+}(M1) sites in hedenbergite, however, the observed h values are not well predicted (see Fig. 7). Therefore, the second approach to interpreting the observed $DE_Q(T)$ curves was attempted. It differs from the previous one in that the full crystal-field Hamiltonian, constructed from point-charge calculations, is used instead of the approximate orthorhombic symmetry (Van Alboom et al. 1993). As such, no simplification of the actual local symmetry of the Fe^{2+} coordination is required. The crystallographic lattice positions of the ions in hedenbergite (Cameron et al. 1973) were used for the FeO_6^{10-} cluster. Since no data are available concerning the charge number of the j^{th} ligand, Z_j, the reported values for diopside (Sasaki et al. 1980) were used as approximate values. Similarly to the first approach, the spin-orbit and Heisenberg-exchange terms were additionally included in the calculations, the latter only at $T < T_N$. The value of 5.25 K was used for the isotropic magnetic-exchange integral. The optimal value for l was determined to be -60 ± 5 cm^{-1}, the same value as estimated in the first approach. The tensor components V_{latq} of the lattice contribution to the EFG were obtained from lattice summations and are indicated in Table 5. According to these calculations, the principal axis of the lattice EFG lies parallel to the crystallographic *b* axis, as required for a site of point symmetry C_2. The main-axis frame of the lattice EFG is rotated approximately –18° around this axis.

In principle, the quantities $<r^2>$, $<r^4>$, and the quadrupole-coupling constant, ΔE_0, appearing in the crystal-field Hamiltonian (Van Alboom et al. 1993) could be evaluated by adjusting the theoretical expressions to the experimental $\Delta E_Q(T)$ curve. However, for the sake of simplicity and for avoiding divergence of the iteration, the radial expectation values $<r^n>$ have been fixed in the iteration procedure. For $<r^4>$, the value calculated from the relation

$$\left\langle r^4 \right\rangle = \Delta_{oct} \frac{3}{5} \frac{a^5}{Ze^2} \qquad (4)$$

was used. In this expression *a* represents the mean M1-O distance and *Ze* the nuclear charge. Taking Δ_{oct} as measured by optical spectroscopy, i.e., 9400 cm^{-1}, one obtains $<r^4> \approx 19.7$ a.u. Keeping $<r^4>$ constant or letting it vary in the iteration has an insignificant effect on the temperature variation of the quadrupole splitting since its value determines the energies of the E_g levels, of which the populations at laboratory temperatures are marginal. For $<r^2>$ the theoretical value of the free Fe^{2+} ion, i.e., 1.39 a.u. (Freeman and Watson 1965) was used. The initial guess for ΔE_0 was the value obtained from the first approach.

The $\Delta E_Q(T)$ curves calculated within the point-charge model do not differ noticeably from those depicted in Figure 4 (solid lines) and are therefore not reproduced. The theoretical $\eta(T)$ variations, however, are much closer to the results extracted from the AFMS (Fig. 8). The agreement is satisfying, considering the estimated experimental error on η and the use of the diopside data concerning ligand charge numbers Z_j. The relevant data are presented in Table 6. The value of η is calculated to be ~0.66 ($T = 80$ K) and coincides within experimental errors ($\pm$ 0.15) with the observed one, viz., $0.70 \le \eta \le 0.80$. Therefore we conclude that this second approach is superior in predicting the EFG features, and hence in evaluating the electronic level scheme of the ^5D orbitals.

It is clear that the calculated positions of the ^5D orbital levels for Fe^{2+} at the M1 site are consistent with the optical transitions Δ_3 and Δ_4 observed by Burns (1993). The energy gaps between the electronic ground state and the two lowest excited states were determined as 405 ± 10 cm^{-1} and 770 ± 20 cm^{-1}, respectively, which are considerably higher than $\Delta_1 = 120$ cm^{-1} and $\Delta_2 = 565$ cm^{-1} as suggested by Stanek et al. (1986). As a result, the temperature variations of the asymmetry parameters

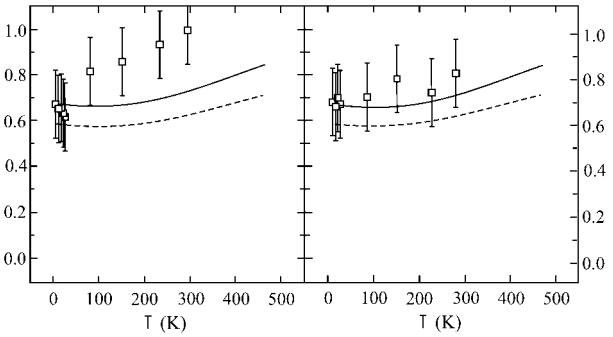

FIGURE 8. Experimental (open box) and calculated (dashed lines) temperature dependence of the asymmetry parameter $\eta(T)$ according to the point-charge model for HED1 (left side) and HED2 (right side). The calculated $\eta(T)$ curves when including the lattice contribution (solid lines) are shown as well.

TABLE 5. Lattice contributions V_{lata} (in units e 10^3 nm^{-3}) to the EFG components of Fe^{2+} at the M1 site in hedenbergite

$$\left[V_{latq}\right] = \begin{bmatrix} 0.0500 & 0.0000 & 0.0165 \\ 0.0000 & -0.0554 & 0.0000 \\ 0.0165 & 0.0000 & 0.0054 \end{bmatrix}$$

TABLE 6. Results concerning the ^5D level scheme and the electric field gradient EFG for Fe^{2+} in HED1 and HED2 as obtained from the temperature variation of the quadrupole splitting based on case 2 of the hypothetical orthorhombic symmetry for the M1 site

Sample	$<r^2>$	$<r^4>$	ΔE_0	α^2	η	Δ_{oct}	Δ_1	Δ_2	Δ_3	Δ_4
HED1	1.98	20.0	3.18	0.84	0.66	9080	410	770	9340	9470
HED2	2.02	20.0	3.18	0.84	0.65	9080	410	790	9350	9490

Notes: Proportionality factors $<r^2>$ and $<r^4>$ (a.u.), quadrupole-coupling constant ΔE_0 (mm/s), covalence factor α^2, asymmetry parameter η at 80 K, cubic level splitting of the ^5D ground term in an octahedral crystal field Δ_{oct} (cm^{-1}), first Δ_1, second Δ_2, third Δ_3, and fourth Δ_4, excited orbital state with respect to the ground state (cm^{-1}).

of HED1 and HED2 are considerably less prominent than suggested by these authors who reported values changing from close to zero at 4.2 K to nearly unity at room temperature. Such a drastic change is hard to reconcile with the observed $\Delta E_Q(T)$ curve. Therefore, it is believed that the values for η as obtained from the present AFMS, i.e., $0.70 \leq \eta \leq 0.80$, are more reliable than those reported earlier in literature, i.e., $\eta < 0.10$ at 4.2 K (Coey and Ghose 1985; Stanek et al. 1986; Regnard and Boujida 1988).

The values obtained for α^2, namely 0.84 (see Table 6), suggest a higher degree of covalence for Fe^{2+}(M1) in hedenbergite as compared to Fe^{2+}(M1) in orthopyroxene, i.e., ≈0.70 (Van Alboom et al. 1993, 1994). The reason for this is, however, not straightforward. It cannot be ascribed to a difference in mean M1-O distance since this distance is very similar for both pyroxene species, viz., 0.213 nm.

In summary, the point-charge-based model calculations for the EFG tensor at the M1 sites in hedenbergite are obviously superior to calculations emanating from a specific approximation for the real point symmetry of the coordination. The same conclusion was arrived at in the case of orthopyroxenes (Van Alboom et al. 1993) and diopsides (see Part III of these studies). Although the computational efforts are at a high level, the authors believe that they are worthwhile, providing valuable information about the electronic level scheme of the ferrous ^5D term, especially about the lowest (T_{2g}) levels for octahedral coordinations in silicates. A crucial prerequisite in this respect is that reliable information from optical spectroscopy must be available. In this way, the above-presented study provides a clear illustration of how two different spectroscopic techniques can give complimentary results.

ACKNOWLEDGMENTS

The authors wish to thank A. Van Alboom for his assistance in programming the computer routines and in carrying out and interpreting the results of the model calculations. They are much indebted to the Fund for Scientific Research–Flanders for the financial support that enabled to carry out the numerous experiments involved in this study.

REFERENCES CITED

Amarasiriwardena, D.D., De Grave, E., Bowen, L.H., and Weed, S.B. (1986) Quantitative determination of aluminum-substituted goethite–hematite mixtures by Mössbauer spectroscopy. Clays and Clay Minerals, 34, 250–256.

Amthauer, G. and Rossman, G.R. (1984) Mixed valence of iron in minerals with cation clusters. Physics and Chemistry of Minerals, 11, 37–51.

Amthauer, G., Lottermoser, W., Redhammer, G., and Tippelt, G. (1998) Mössbauer studies of selected synthetic silicates. Hyperfine Interactions, 113, 219–248.

Bancroft, G.M., Williams, P.G.L., and Burns, R.G. (1971) Mössbauer spectra of minerals along the diopside-hedenbergite tie line. American Mineralogist, 56, 1617–1625.

Baum, E., Treutmann, W., Lottermoser, W., and Amthauer, G. (1997) Magnetic properties of the clinopyroxenes aegirine and hedenbergite: a magnetic susceptibility study on single crystals. Physics and Chemistry of Minerals, 24, 294–300.

Burns, R.G. (1993) Mineralogical applications of crystal field theory (2nd edition). 551 p., Cambridge University Press, Cambridge.

Cameron, M., Sueno, S., Prewitt, C.T., and Papike, J.J. (1973) High-temperature crystal chemistry of acmite, diopside, hedenbergite, jadeite, spodumene, and ureyite. American Mineralogist, 58, 594–618.

Chambaere, D. and De Grave, E. (1984) On the Néel temperature of β-FeOOH: structural dependence and its implications. Journal of Magnetism and Magnetic Materials, 42, 263–268.

Coey, J.M.D. and Ghose, S. (1985) Magnetic order in hedenbergite: $CaFeSi_2O_6$. Solid State Communications, 53, 143–145.

Collins, R.L. and Travis, J.C. (1967) The electric field gradient tensor. In I.J. Gruverman, Ed., Mössbauer Effect Methodology 3, p. 123–161. Plenum Press, New York.

De Grave, E. and Van Alboom, A. (1991) Evaluation of ferrous and ferric Mössbauer fractions. Physics and Chemistry of Minerals, 18, 337–342.

De Grave, J., De Paepe, P., De Grave, E., Vochten, R., and Eeckhout, S.G. (2002) Mineralogical and Mössbauer spectroscopic study of a diopside occurring in the marbles of Andranondamo, southern Madagascar. American Mineralogist, 87, 132–141.

Dollase, W.A. and Gustafson, W.I. (1982) ^{57}Fe Mössbauer spectral analysis of the sodic clinopyroxenes. American Mineralogist, 67, 311–327.

Dowty, E. and Lindsley, D.H. (1973) Mössbauer spectra of synthetic hedenbergite-ferrosilite pyroxenes. American Mineralogist, 58, 850–868.

Eeckhout, S.G., De Grave, E., McCammon, C.A., and Vochten, R. (2000) Temperature dependence of the hyperfine parameters of synthetic $P2_1/c$ Mg-Fe clinopyroxenes along the $MgSiO_3$-$FeSiO_3$ join. American Mineralogist, 85, 943–952.

Freeman, A.J. and Watson, R.E. (1965) Hyperfine interactions in magnetic materials. In G.T. Rado, and H. Suhl, Eds., Magnetism IIA, p. 167–305. Academic Press, New York.

Ghose, S., Hewat, A.W., Van Dang, N., and Weidner, J.R. (1988) Magnetic phase transitions in quasi-one dimensional antiferromagnets: ferrosilite, $Fe_2Si_2O_6$, and hedenbergite, $CaFeSi_2O_6$. Materials Science Forum, 27/28, 235–242.

Ingalls, R. (1964) Electric-field gradient tensor in ferrous compounds. Physical Review, 133, A787–A795.

Morimoto, N. (1988) Nomenclature of pyroxenes. American Mineralogist, 73, 1123–1133.

Morrish, A.H. (1965) The physical principles of magnetism. 680 p. Wiley, New York.

Nagy, D.L. (1978) Deformation-induced texture in Mössbauer absorbers. Applied Physics, 17, 269–274.

Perkins, H.K. and Hazony, Y. (1972) Temperature-dependent crystal field and charge density: Mössbauer studies of FeF_2, $KFeF_3$, $FeCl_2$ and FeF_3. Physical Review, B5, 7–18.

Redhammer, G.J., Amthauer, G., Lottermoser, W., and Treutmann, W. (2000) Synthesis and structural properties of clinopyroxenes of the hedenbergite $CaFe^{2+}Si_2O_6$–aegirine $NaFe^{3+}Si_2O_6$ solid-solution series. European Journal of Mineralogy, 12, 105–120.

Regnard, J.R. and Boujida, M. (1988) Relations between magnetic hyperfine field distribution and cation order in natural hedenbergite. Hyperfine Interactions, 41, 513–516.

Sasaki, S., Fujino, K., Takéuchi, Y., and Sadanaga, R. (1980) On the estimation of atomic charges by X-ray method for some oxides and silicates. Acta Crystallographica, A36, 904–915.

Seifert, F. (1983) Mössbauer line broadening in aluminous orthopyroxenes: Evidence for next nearest neighbors interactions and short-range order. Neues Jahrbuch für Mineralogie Abhandlungen, 148, 141–162.

Stanek, J., Hafner, S.S., Regnard, J.R., and El Goresy, J. (1986) Temperature-dependent hyperfine parameters in $CaFeSi_2O_6$. Hyperfine interactions, 28, 829–832.

Tennant, W.C., McCammon, C.A., and Miletich, R. (2000) Electric-field gradient and mean-squared-displacement tensors in hedenbergite from single-crystal Mössbauer milliprobe measurements. Physics and Chemistry of Minerals, 27, 156–163.

Van Alboom, A. and De Grave, E. (1996) Temperature dependence of the ^{57}Fe Mössbauer parameters in riebeckite. Physics and Chemistry of Minerals, 23, 377–386.

Van Alboom, A., De Grave, E., and Vandenberghe, R.E. (1993) Study of the temperature dependence of the hyperfine parameters in two orthopyroxenes by ^{57}Fe Mössbauer spectroscopy. Physics and Chemistry of Minerals, 20, 263–275.

———(1994) Crystal-field interpretation of the temperature dependence of the ^{57}Fe Mössbauer quadrupole splitting in two orthopyroxenes. Hyperfine Interactions, 91, 703–707.

Vandenberghe, R.E., De Grave, E., and de Bakker, P.M.A. (1994) On the methodology of the analysis of Mössbauer spectra. Hyperfine Interactions, 83, 29–49.

Varret, F. (1976a) Mössbauer spectra of paramagnetic powders under applied field: Fe^{2+} in fluosilicates. Journal of Physics and Chemistry of Solids, 37, 265–271.

——— (1976b) Crystal-field effects on high-spin ferrous iron. Journal de Physique Colloque C6, 37, 437–456.

Wiedenmann, A. and Regnard, J.R. (1986) Neutron diffraction study of the magnetic ordering in pyroxenes $Fe_xM_{1-x}SiO_3$. Solid State Communications, 57, 499–504.

Wivel, C.O. and Mørup, S. (1981) Improved computational procedure for evaluation of overlapping hyperfine parameter distributions in Mössbauer spectra. Journal of Physics E: Scientific Instruments, 14, 605–610.

MANUSCRIPT RECEIVED APRIL 2, 2002
MANUSCRIPT ACCEPTED NOVEMBER 15, 2002
MANUSCRIPT HANDLED BY DARBY DYAR